ARTICLES
PUBLISHED ONLINE: 23 JULY 2010 | DOI: 10.1038/NMAT2811
nature materials

Quantum-dot/dopamine bioconjugates function as redox coupled assemblies for *in vitro* and intracellular pH sensing

Igor L. Medintz[1]*, Michael H. Stewart[2], Scott A. Trammell[1], Kimihiro Susumu[2], James B. Delehanty[1], Bing C. Mei[2,3], Joseph S. Melinger[4], Juan B. Blanco-Canosa[5], Philip E. Dawson[5] and Hedi Mattoussi[2]†

The use of semiconductor quantum dots (QDs) for bioimaging and sensing has progressively matured over the past decade. QDs are highly sensitive to charge-transfer processes, which can alter their optical properties. Here, we demonstrate that QD–dopamine–peptide bioconjugates can function as charge-transfer coupled pH sensors. Dopamine is normally characterized by two intrinsic redox properties: a Nernstian dependence of formal potential on pH and oxidation of hydroquinone to quinone by O_2 at basic pH. We show that the latter quinone can function as an electron acceptor quenching QD photoluminescence in a manner that depends directly on pH. We characterize the pH-dependent QD quenching using both electrochemistry and spectroscopy. QD–dopamine conjugates were also used as pH sensors that measured changes in cytoplasmic pH as cells underwent drug-induced alkalosis. A detailed mechanism describing the QD quenching processes that is consistent with dopamine's inherent redox chemistry is presented.

Semiconductor QDs have become well-established photoluminescent (PL) platforms for biological applications[1,2]. Unlike most organic dyes, QDs are also highly sensitive to charge transfer, which can alter their optical properties[3,4], thus generating interest in charge-transfer-based biosensing[5]. Redox-active compounds including metal complexes, ions and dyes have already been investigated for use in photoinduced electron-transfer QD biosensing[6–12]. Catechols have also undergone extensive testing with QDs owing to their interesting electrochemistry, and differing interpretations have been used to explain the disparate results. Progressive quenching of CdSe/ZnS (ref. 13), CdS:Mn/ZnS (ref. 14), CdSe (ref. 15), CdTe (refs 16,17) and CdS (ref. 18) QDs in the presence of increasing benzoquinones and dopamine has been most commonly reported where the quinone is suggested as an electron acceptor. A mechanism whereby dopamine increases the rate of quenching through Förster resonance energy transfer (FRET) has also been postulated[18]. In contrast, PL increases of CdSe/CdS QDs in the presence of benzoquinone[19] along with both CdSe/ZnS (ref. 20) and CdTe (ref. 21) QDs by dopamine have also been found. Nadeau and co-workers reported that QD–dopamine bioconjugates can stain dopamine-receptor-expressing cells in redox-sensitive patterns where increased fluorescence was noted under oxidizing conditions[20]. Dopamine was suggested here as an electron donor that could quench or sensitize QDs through different mechanisms involving reactive oxygen[20,21]. Cumulatively, this confirms a role for quinones and especially dopamine in redox interactions with QDs; however, a full understanding of this system and how to exploit it for biosensing is lacking.

Using peptides covalently displaying dopamine-hydroquinone controllably self-assembled onto QDs, we demonstrate that PL quenching arises from a pH-dependent electron-transfer process from QDs to oxidized dopamine-quinone functioning as an electron acceptor (see Fig. 1a,b). Following photoexcitation, the QD conduction-band electron is transferred to the lowest unoccupied molecular orbital of a quinone acceptor, resulting in PL quenching, and the electron is then shuttled back to the QD valence band (see below). The pH-dependent concentration of oxidized dopamine in the QD conjugate at any point determines the magnitude of electron transfer and concomitant QD PL quenching. At low pH, the concentration of oxidized dopamine is small producing only marginal quenching. As pH increases, dopamine undergoes a proportional increase in oxidation to quinone by ambient O_2 and the appearance of this electron acceptor near the QD provides a favourable non-radiative channel for increased QD quenching as verified by shortening of the QD exciton lifetime. We show PL quenching efficiency to be dependent on QD size, as more pronounced quenching was observed for smaller-sized QDs. This arises as decreasing nanocrystal size provides better spatial overlap of carriers and a larger driving force, enhancing the probability of electron transfer.

This mechanism is consistent with the electrochemistry of dopamine and structurally related quinone molecules, which are known potent electron acceptors in biological and abiotic formats[22–24]. As with other hydroquinones, dopamine undergoes autoxidation and is also oxidized by molecular O_2, generating a concomitant H_2O_2 species. Such coupled electron–proton systems exhibit slow redox kinetics with rate constants in aqueous solution that directly depend on pH (refs 22,25). Rates of oxidation to quinone increase markedly in buffers by >1,000-fold as pH increases from 6 to 12 (refs 22,24,26).

[1]Center for Bio/Molecular Science and Engineering Code 6900, US Naval Research Laboratory, Washington, District of Columbia 20375, USA, [2]Optical Sciences Division Code 5611, US Naval Research Laboratory, Washington, District of Columbia 20375, USA, [3]Department of Chemical Engineering, University of Massachusetts, Amherst, Massachusetts 01003, USA, [4]Electronic Science and Technology Code 6812, US Naval Research Laboratory, Washington, District of Columbia 20375, USA, [5]Departments of Cell Biology & Chemistry, The Scripps Research Institute, La Jolla, California 92037, USA.
†Present address: Department of Chemistry and Biochemistry, Florida State University, Tallahassee, Florida 32306, USA.
*e-mail: igor.medintz@nrl.navy.mil.

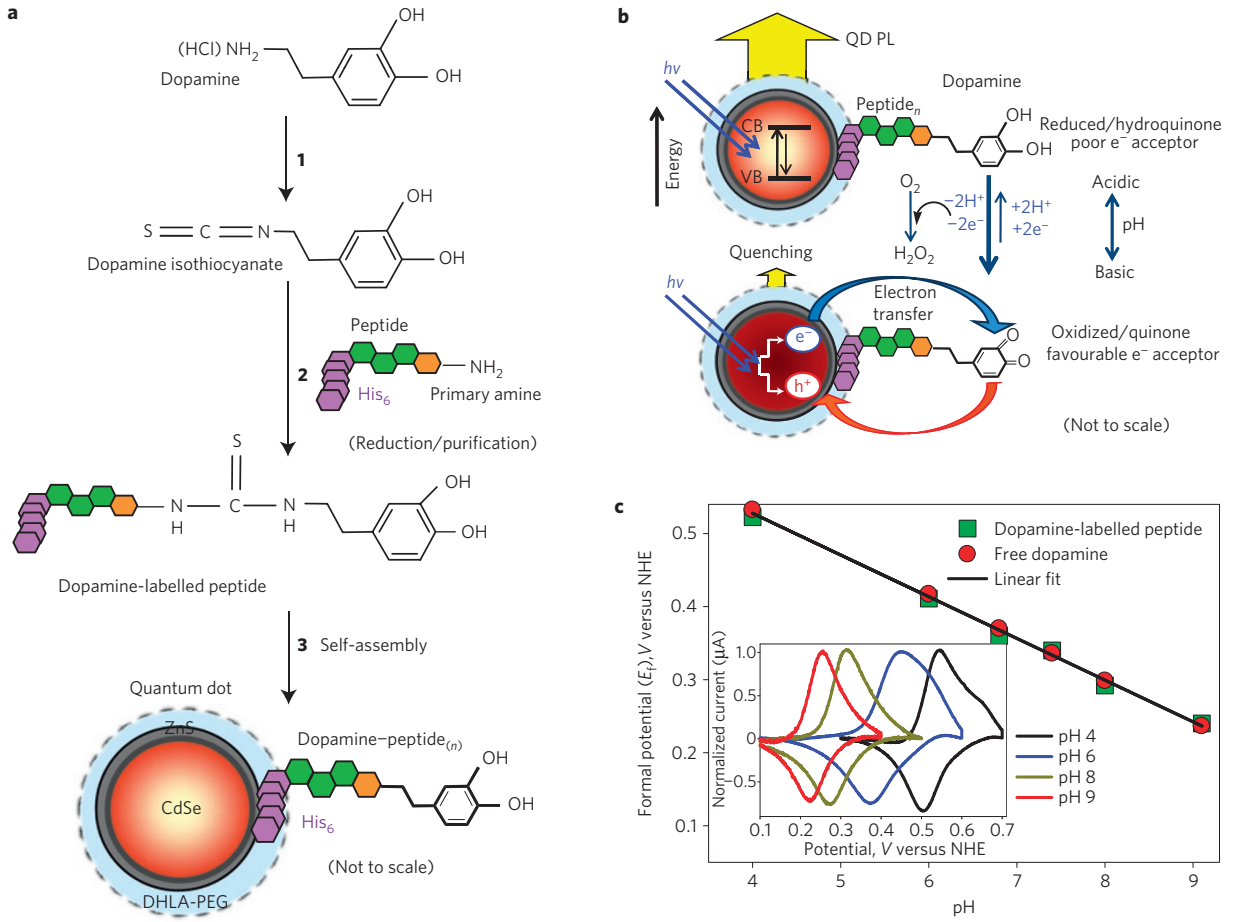

Figure 1 | Dopamine–peptide synthesis, QD conjugation, energy-transfer mechanism and cyclic voltammetry. a, Step 1: dopamine is activated to an amine-reactive isothiocyanate. Step 2: the unique primary amine on the peptide is site-specifically modified with dopamine isothiocyanate. The peptide is then reduced with hydrazine and purified. Step 3: dopamine–peptide is ratiometrically self-assembled to DHLA-PEG QDs through the $(His)_6$ sequence. **b**, Peptides with dopamine pre-reduced to hydroquinone are self-assembled to QDs. Only one is shown for brevity. At low pH, hydroquinone is predominant and as a poor electron acceptor this results in low QD PL quenching. As pH increases, ambient O_2 in the buffer oxidizes dopamine, producing a hydrogen peroxide (H_2O_2) species. The increasing quinone concentration provides favourable electron acceptors in close proximity to the QD. This produces higher quenching efficiencies with a magnitude directly proportional to the amount of quinone. The orange arrow indicates the probability of the electron shuttling back to the QD valence band (VB). CB = conduction band. **c**, Plot of dopamine and dopamine–peptide formal potential E_f versus pH highlighting the linear Nernstian response. Inset: Cyclic voltammograms of dopamine–peptide collected in different pH buffers at a 50 mV s^{-1} scan rate. More details on QD and dopamine–peptide synthesis along with the electrochemistry can be found in the Methods section and the Supplementary Information. NHE is normal hydrogen electrode.

The protonation states of dopamine's 2-hydroxyl groups (p*K*a values 9.3, 12.6) also change as a function of pH, directly affecting electrochemistry. Dopamine's pH-dependent electron–proton coupled redox mechanisms are exceedingly complex and beyond the present scope: the multiple steps are best described by Laviron's scheme (see Supplementary Information)[22]. This complexity makes it hard to predict the exact amount of hydroquinone/quinone present at any one pH point in our QD–dopamine–peptide system. We pre-reduce dopamine–peptide before assembly onto QDs, ensuring that dopamine is in the hydroquinone form until pH changes are used to induce oxidation to quinone (see the Methods section). Combining this factor with control over the QD/dopamine ratio afforded by our peptide self-assembly approach makes this system far more tractable to analysis.

We began by confirming that dopamine-labelled peptide retains the same electrochemistry as unmodified dopamine because the isothiocyanate functionality used for peptide attachment is not on the redox-active catechol ring (see Fig. 1a). Dopamine exhibits a Nernstian response for a two-electron, two-proton redox couple producing a linear change in formal potential (E_f, average anodic/cathodic peak potentials) versus pH with a slope of ~59 mV per pH unit. This originates from catechol electochemistry, as predicted by the modified Nernst equation[27]:

$$E_f = E^o - 0.059(h/n)(\mathrm{pH})$$

where E^o is the potential at pH 0 and h/n designates the ratio of protons and electrons, respectively[27]. E_f shifts to negative values at higher pH owing to decreasing protons. Figure 1c plots changes in E_f (slope ~59 mV per pH unit) from dopamine/dopamine–peptide measured at glassy carbon electrodes in buffers of increasing pH (full pH range 4–13, see Supplementary Information). Normalized cyclic voltammograms from dopamine–peptide are shown in the inset. As pH increases from 4 to 9, cyclic voltammograms undergo a consistent shift in anodic and cathodic peak to lower potential, identical to the process observed for free dopamine[24–29]. Only a single pair of oxidation/reduction peaks was observed in this system, typical of cyclic voltammograms measured in buffer where individual electron-transfer steps overlap[29]. This result is

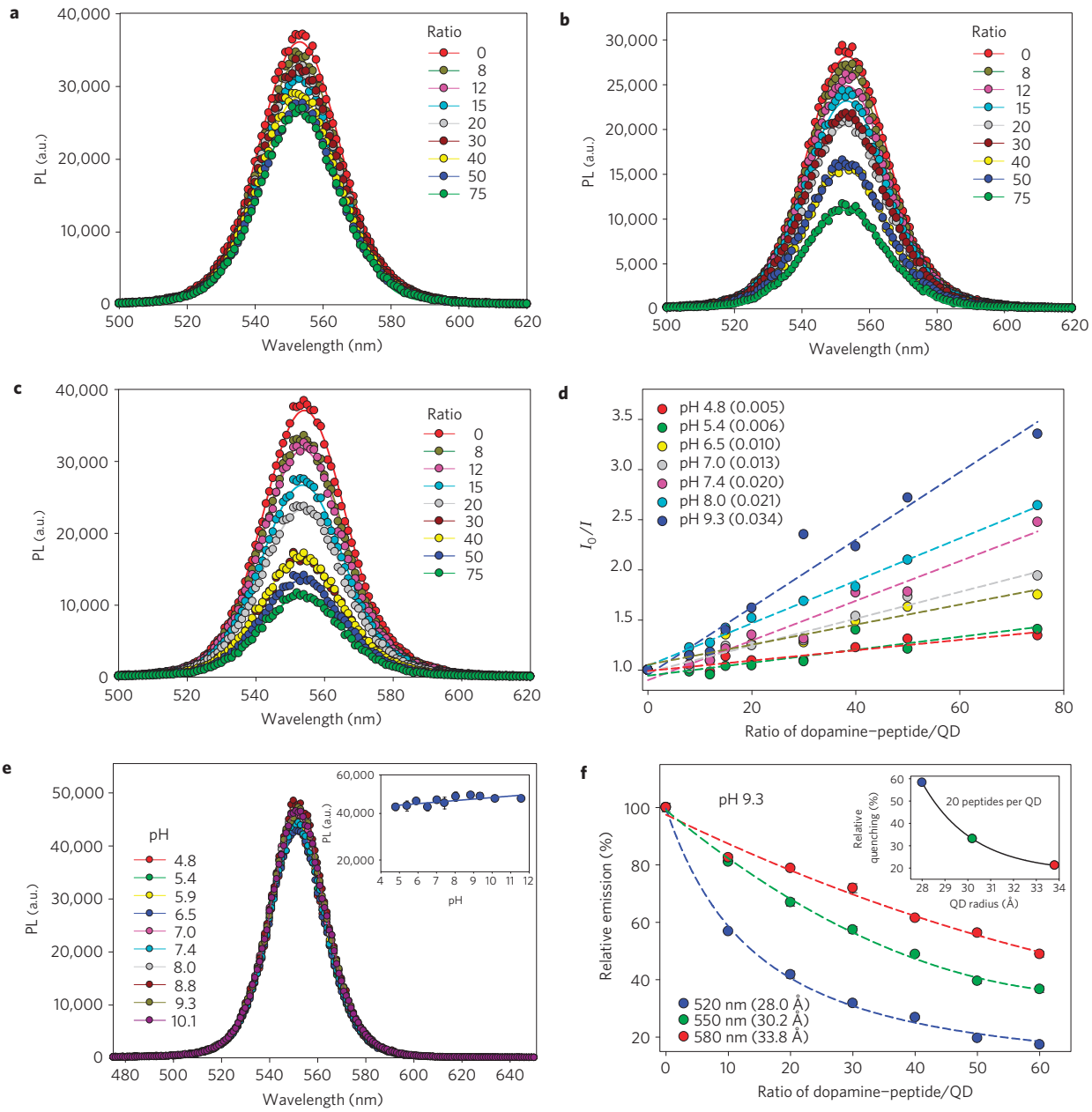

Figure 2 | Steady-state photoluminescence spectra. a–c, Representative PL spectra collected from 550-nm-emitting QDs self-assembled with an increasing ratio of dopamine–peptide added to PBS buffer at pH 4.8 (**a**), pH 7.4 (**b**) and pH 9.3 (**c**). Spectra were collected on a Tecan Safire dual monochromator multifunctional microtitre plate reader with 350 nm excitation. QD PL spectra were fitted with a Gaussian profile. **d**, Plots of increasing ratio of dopamine–peptide/QD versus pH in a Stern–Volmer format (I_0/I versus ratio of dopamine/QD). Values in parenthesis are slopes derived for each data set reflecting the higher quenching versus ratio for increasing pH values. **e**, PL spectra of control 550 nm QD in the absence of dopamine–peptide in the different pH buffers. Inset: Plot of QD PL at 550 nm versus pH. Standard deviations (s.d.) calculated from at least three replicate sample are shown. **f**, Normalized quenching of 520-nm, 550-nm and 580-nm-emitting QDs assembled with increasing dopamine–peptide and exposed to pH 9.3 buffer. Inset: Relative quenching versus QD core/shell radius for 20 peptides per QD valence (520 nm ~ 28 Å, 550 nm ~ 30.2 Å, 580 nm ~ 33.8 Å, assuming 4–5 monolayers of ZnS shell)[60]. Lines of best fit are shown.

analogous to previous ones where a protein was similarly modified with benzoquinone[30].

We monitored the effects of attaching increasing ratios (valence) of dopamine–peptides to QDs while varying pH. Analysing self-assembled QD–peptide conjugates indicated that on average ~50–60 peptides could be maximally assembled to these QDs (ref. 31); thus, a slight excess of 75 peptides per QD was the highest valence tested to assure full coverage. Figure 2a–c shows PL spectra collected from 550-nm-emitting QDs self-assembled with increasing dopamine–peptide at pH 4.8, 7.4 and 9.3 (see extra plots in Supplementary Fig. S2). Figure 2d presents results across seven pH values in a Stern–Volmer format allowing direct comparison of both valence and pH. Two simultaneous processes become apparent: at a given pH, QD quenching increases as a function of dopamine ratio and the relative magnitude of quenching substantially increases with basic pH. Maximal quenching is rapidly reached after conjugate addition to buffer and no further increases were seen within our experimental time frames (3–5 h). Similar quenching trends were observed with 520- and 580-nm-emitting QDs (see below).

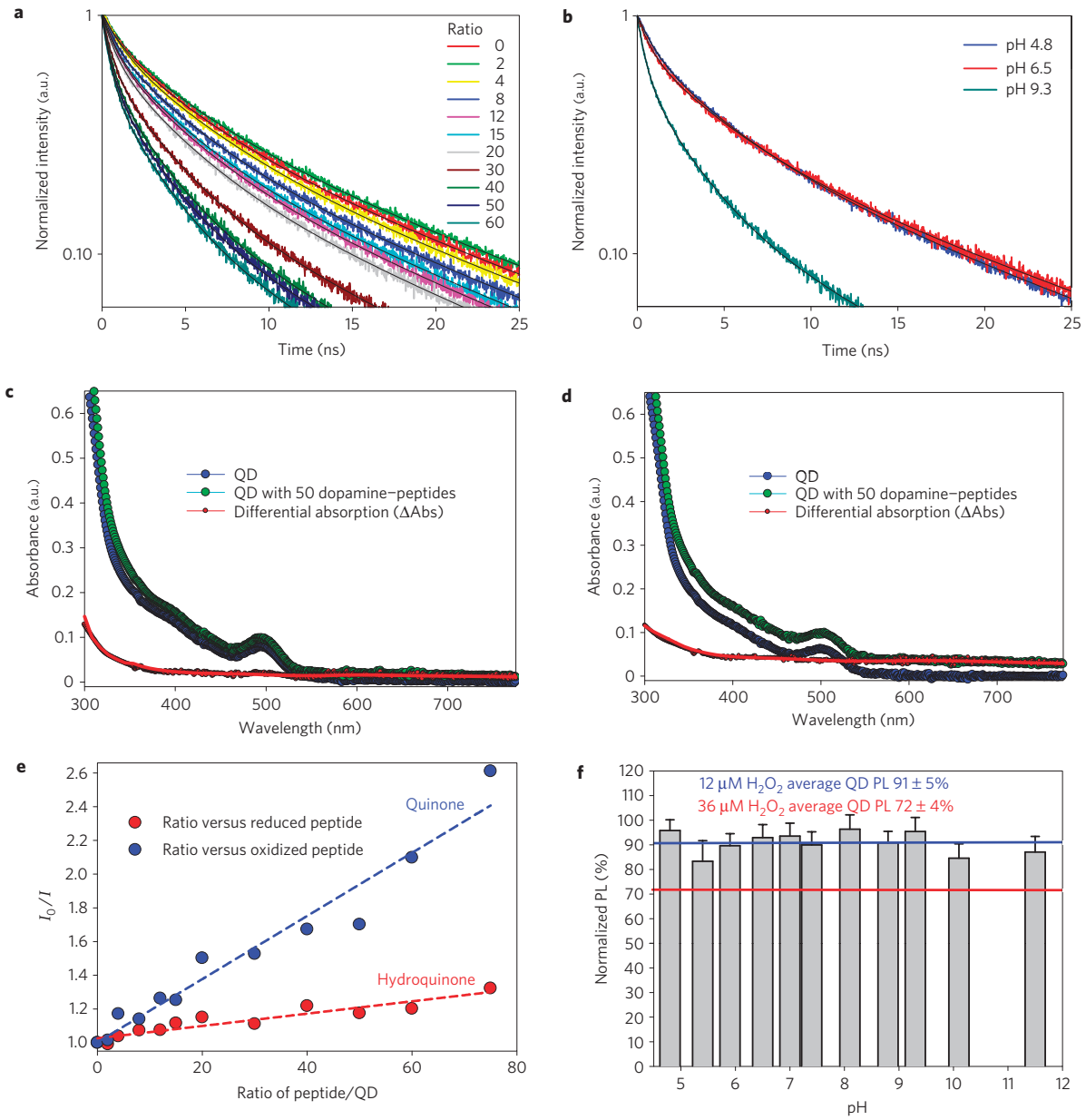

Figure 3 | Excited-state lifetimes, QD absorption, oxidation and H_2O_2. **a**, Representative, normalized time-resolved PL decays of 550-nm-emitting QDs self-assembled with indicated ratios of dopamine–peptides in PBS pH 9.3. **b**, Normalized PL decays from 550-nm QDs assembled with 50 dopamine–peptides per QD at pH 4.8, 6.5 and 9.3. **c**,**d**, Absorption spectra collected from 550-nm QDs and QD–dopamine conjugates at pH 4.8 (**c**) and pH 9.3 (**d**). Differential absorption (ΔAbs) for each is plotted in red. No significant absorption was noted for dopamine–peptide-only controls at the same pH values in this spectral window. **e**, Representative quenching data (I_0/I versus dopamine/QD ratio) for 550 nm QDs self-assembled with dopamine–peptide pre-reduced (hydroquinone) or pre-oxidized (quinone). The samples were tested at pH 6 to keep the hydroquinone in reduced form. **f**, 580-nm QDs incubated with H_2O_2 at various pH values and resultant PL normalized to that of controls in the same buffer without H_2O_2. The blue (12 μM H_2O_2) and red (36 μM H_2O_2) lines are the average QD PL across all pH values obtained for each H_2O_2 concentration tested. The concentrations simulate the maximal amount of H_2O_2 potentially generated in our system and three-times that value.

Control experiments using QDs dispersed in the same buffers (see Fig. 2e) or QDs self-assembled with unlabelled peptides showed no effects on PL (data not shown). To confirm that quenching was being mediated by dopamine assembly and not collisional interactions, we compared these results with experiments carried out with free dopamine (see Supplementary Fig. S3). Significant QD quenching (>20%) was not seen with free dopamine until pH 7 or higher and then with a 40,000-fold excess compared with the molar equivalent of dopamine–peptide used. Effects of QD size on quenching were also examined. Figure 2f compares normalized emission from three different QD sizes when assembled with increasing dopamine–peptide at pH 9.3. The inset shows quenching efficiency versus QD radius for 20 dopamines per QD. Although similar quenching trends versus dopamine valence are noted in all samples, a threefold reduction in quenching efficiency is noted as QD radius increases by ~20%.

Figure 3a presents time-resolved PL decays from 550-nm QDs assembled with increasing dopamine–peptide at pH 9.3 where a significant, progressive decrease in exciton lifetime is measured with increasing dopamine. In Fig. 3b, we compare the effects of varying pH on the QD PL decay for QDs conjugated to 50 dopamine–peptides. Data show that under acidic pHs of 4.8 and

6.5, no significant changes in QD exciton lifetime are noted as compared to pH 9.3 (see Supplementary Fig. S4 and Table S1). Absorption spectra of 550-nm QDs with/without 50 dopamine–peptides per QD were measured at pH 4.8 and pH 9.3 representing minimum and strong PL quenching conditions, respectively (see Fig. 3c,d). The red line in each plot is the differential absorption (ΔAbs) obtained from subtracting QD–dopamine–peptide absorption from the native QD spectra[3,8]. Although a small background wavelength-independent contribution is seen at higher pH resulting from oxidized dopamine[32], no significant differences in ΔAbs are noted.

Further experiments focused on confirming that dopamine oxidation is responsible for the QD quenching observed. The first probed whether dopamine adducts do undergo pH-dependent oxidation to quinone by O_2. Dopamine was coupled by its amine to a short polyethylene glycol (PEG) molecule (preventing cyclization and removing the peptide's ultraviolet absorption) and changes in absorption were monitored with increasing pH (see Supplementary Fig. S5). Similar to what was observed for pH-induced oxidation of free dopamine[32], changes in absorption were noted only at basic pH (>pH 7) as quinone formed during initial incubation. Second, degassing buffers with Ar to remove O_2 before QD–dopamine conjugate addition reduced quenching significantly by >70% across all pH values (data not shown). Third, bringing quinone alone in proximity to the QD should be sufficient to induce quenching without pH changes. We thus carried out side-by-side PL comparisons of 550-nm QDs assembled with dopamine–peptide either pre-reduced (hydroquinone) or alternatively pre-oxidized (quinone) by H_2O_2 during purification. Samples were tested at pH 6 to keep the hydroquinone reduced. As summarized in Fig. 3e, significantly higher quenching (∼×2.5 more) was measured for conjugates assembled with pre-oxidized dopamine, confirming that quinone proximity alone is sufficient to quench QD PL. Last, H_2O_2 itself can quench QDs, although the mechanism(s) remains unclear, that is, electron removal or 'oxidative' etching[33–35]. We estimated the maximum H_2O_2 generated in our conjugates, assuming stoichiometric correspondence with dopamine, and tested it for QD quenching. This elicited only a ≤10% quenching of the QDs and a further threefold increase in H_2O_2 increased quenching to only ∼28%; all independent of pH (see Fig. 3e). Moreover, H_2O_2 is unstable and rapidly decomposes at high pH where most quenching occurs[36]. Last, samples were excited at 350 nm (dopamine absorption minima) and conjugates were repeatedly photoexcited >25 consecutive times without loss of QD quenching even after several days (data not shown). This suggests that neither H_2O_2 oxidation nor dopamine photo-oxidation are primary QD quenching mechanisms.

We tested the conjugates' ability to measure pH changes by monitoring the PL progression from 550 nm QD–dopamine conjugates side-by-side with a 680 nm red-fluorescent Fluorophorex 20 nm nanosphere internal standard (abbreviated FLX). Figure 4a shows spectra from conjugates (60 dopamines per QD) dispersed in increasing pH together with FLX. As pH increased from 6.5 to 11.5, QD PL decreased ∼70% whereas FLX is essentially unchanged (≤10%). The inset shows PL loss normalized to pH 6.5 values for both QD conjugates and FLX over the pH range. The ratio of PL intensities for FLX and QDs versus pH is plotted in Fig. 4b superimposed over dopamine–peptide E_f versus pH. Significantly, the response of the PL ratios and E_f slopes versus pH are both linear. Similar results were also obtained with 550-nm and 580-nm QDs mixed with a Cy5 internal standard (see Supplementary Fig. S6). Changes in solution pH could also be monitored with time-resolved measurements, as highlighted in Fig. 4c. We also tested QD-conjugate ability to sense pH changes in the reverse, decreasing pH configuration. Solutions of 550-nm QD–dopamine conjugates were prepared in pH 10.1 buffer (prequenched), and diluted into buffers decreasing from pH 10.1 to 4.8. Figure 4d shows spectra where the conjugates exhibit a pH-dependent factor of two increase in PL, although the strongest PL recovery was lower than that of unquenched QDs.

Last, we evaluated whether QD–dopamine sensing could monitor intracellular pH changes. Effects of the polyene antifungal drug nystatin on eukaryotic cells were used to test the QD conjugates. Nystatin binds ergosterol in fungal cellular membranes, forming pores that lead to ionic leakage and death. As ergosterol is unique to fungi, the drug is innocuous to eukaryotic cells at low concentrations; however, at higher concentrations nystatin creates molecular-scale pores that do not diffuse and allow only H^+/OH^- ions to be exchanged with the extracellular environment[37]. We used nystatin to induce pores in the membrane of COS-1 cells microinjected with QD–dopamine conjugates and monitored the progressive change in cytosolic pH to that of the medium. In essence, we exploit the cells as a model system into which we sequester sensors and control pH through nystatin effects on the membrane. Cells were microinjected with 550-nm QD conjugates (60 dopamines per QD, 5 μM) premixed with 0.001% FLX in PBS pH 6.5. Growth medium was switched to PBS pH 11.5 supplemented with/without nystatin and micrographs collected regularly using constant exposure settings (see Fig. 5a). A steady decrease in cytoplasmic QD PL in the presence of nystatin was observed (FLX remained constant) as equilibrium was reached between cytosolic pH and surrounding medium, whereas the overall cellular morphology appeared unperturbed during the ∼1 h experiments. Fluorescence from each cell over time was analysed using NIH Image J software. Initial PL signals from the QD–dopamine conjugates and FLX at pH 6.5 were normalized to 100% and subsequent PL signals from both channels versus time are plotted in Fig. 5b. Figure 4b data were used as a calibration curve and the resulting time-dependent pH traces for all cells (and the individual cell outlined in Fig. 5a) are plotted in Fig. 5c. Negligible quenching (≤10%) of QD-conjugate PL was noted in cells lacking nystatin even after 2 h exposure to basic medium (see Supplementary Fig. S7). Carrying out the same experiments using cells preloaded with the pH-sensing dye BCECF confirmed that nystatin facilitates intracellular alkalosis (see Supplementary Fig. S8). QD PL losses in nystatin-exposed cells do not result from photobleaching, as conjugates microinjected in cells showed insignificant PL changes under continuous ultraviolet illumination after several minutes of maximal exposure (see Supplementary Fig. S9). QD–dopamine conjugates could also transduce intracellular pH decreases, although PL recovery was not as significant as quenching observed with pH increases (see Supplementary Fig. S10).

These results can be summarized as follows. (1) Attaching dopamine to a peptide by its amine does not alter its electrochemistry; linear E_f versus pH of dopamine/dopamine–peptide are superimposable (see Fig. 1c). (2) Bringing dopamine in proximity to the QD through peptide self-assembly quenches PL in a manner proportional to dopamine valence and (3) also depends on pH, with higher quenching measured in basic compared with acidic. (4) pH-dependent quenching of QD–dopamine conjugates was significantly enhanced compared with QDs mixed with free dopamine. (5) Quenching manifests with a concurrent shortening of QD exciton lifetime and (6) is dependent on QD size. (7) QD conjugates exhibit a linear dependence of quenching efficiency versus pH similar to that exhibited by dopamine E_f (see Fig. 4b). (8) At each pH/valence tested, maximal quenching is rapidly reached after conjugate addition. (9) Negligible changes in ΔAbs are measured when QDs are significantly quenched by dopamine–peptide at basic pH (see Fig. 3c,d). This contrasts with results where QDs were assembled with a peptide-labelled Ru-electron donor complex[8]. There, significant bleaching of the QD absorption together with a

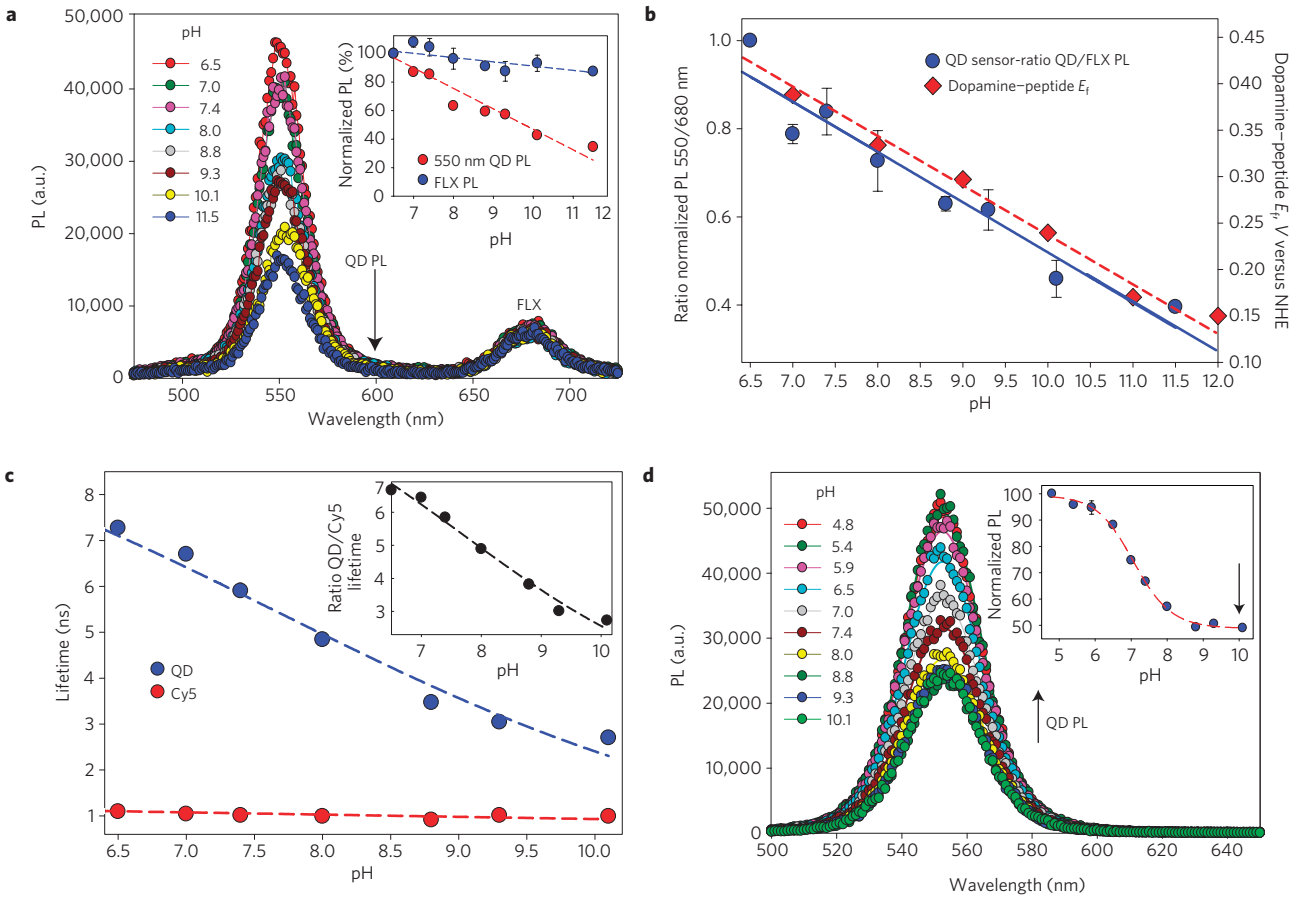

Figure 4 | pH sensing *in vitro*. **a**, Spectra collected from 550-nm-emitting QD–dopamine conjugates mixed with FLX nanospheres at increasing pH values ranging from 6.5 to 11.5. Inset: PL normalized to initial values at pH 6.5 as percentages. **b**, Ratio of normalized QD PL at 550 nm/FLX PL at 680 nm derived from **a**, with a linear fit superimposed over a plot of dopamine–peptide formal potential E_f. Note, this was used as a calibration curve in Fig. 5. **c**, Plot of the averaged excited-state lifetimes derived from QD–dopamine conjugates along with Cy5 dye at the indicated pH values. QDs demonstrate a progressive decrease in average lifetime from 7.27 to 2.70 ns (~75%), whereas a consistent average lifetime of 1.01±0.05 ns is collected from the Cy5 dye (see Supplementary Table S2). Inset: The ratio of QD to Cy5 lifetime versus pH derives a similar linear function as steady-state data and confirms that sensing can be effectively accomplished using both steady-state and time-resolved measurements. **d**, PL spectra collected from 550 nm QDs self-assembled with 50 dopamine-labelled peptides per QD prequenched in pH 10.1 buffer and then added to decreasing pH buffers. Inset: Plot of the PL increase starting from pH 10.1 (arrow) and normalized to pH 4.8.

wavelength-dependent, red-tailing contribution was noted in the ΔAbs because of electron injection into the QDs (ref. 8). (10) QD quenching by dopamine cannot be explained by Förster coupling because of a lack of spectral overlap[32,38].

These data are all consistent with the mechanism we initially outlined (see Fig. 1b) and studies showing quinones to be electron acceptors for QDs. Using a similar peptidyl system, Willner and co-workers demonstrated that tyrosinase can quench aqueous CdSe/ZnS QDs by enzymatically modifying the terminal tyrosine on a QD-attached peptide to L-3,4-dihydroxyphenylalanine (L-DOPA), which underwent subsequent oxidation to an *o*-quinone electron acceptor[13]. Addition of thrombin cleaved the quinone portion of the peptide, producing a QD PL recovery that tracked enzyme concentration. A later study confirmed that tyrosinase modification of tyrosine to a quinone could also quench CdTe core-only QDs (ref. 35). Mirroring our results with pre-oxidized dopamine–peptide (see Fig. 3e), quinone presence alone in these systems is sufficient to quench QDs. Similar results have also been observed for CuS, CdSe and CdSe/ZnS QDs exposed to quinones in organic systems[39–42]. Burda *et al.* demonstrated that when adsorbed to CdSe core-only QDs, 1,4-benzoquinone and 1,2-naphthoquinone functioned as effective electron acceptors for the photoexcited QD conduction-band electron[39]; a result confirmed by others[42]. Burda *et al.* further showed that the quinone shuttles the electron to the hole in the valence band at a rate far quicker than inherent electron–hole recombination. Forward electron transfer from reduced dopamine to the hole in the QD valence band generated on photoexcitation may be an alternative quenching mechanism. Energy-level mismatch as dopamine E_f decreases with increasing pH seems to suggest this possibility. Several lines of evidence, however, argue against this forward transfer. First, QD assembly with pre-oxidized/reduced dopamine peptides at pH 6 would have produced a different outcome; the hydroquinone–peptide would have manifested far stronger quenching than the quinone as it is favoured to donate electrons here. Second, electron transfer from dopamine to the QD should translate into significant changes in the QDs' absorption spectra that were not observed[8]. Third, at basic pH there is significantly less hydroquinone present although the QDs are far more quenched. Last, estimates of electron-transfer driving force between QDs and hydroquinone as a function of pH using the Rehm–Weller model indicate forward electron transfer to be unfavourable (see Supplementary Information).

Spectroscopic data confirm that QD-conjugate quenching begins at ≥pH 7 and extends well into the basic, reflecting the point where dopamine oxidation rates in buffer increase[25,26] and quinone presence becomes significant enough for effective electron transfer.

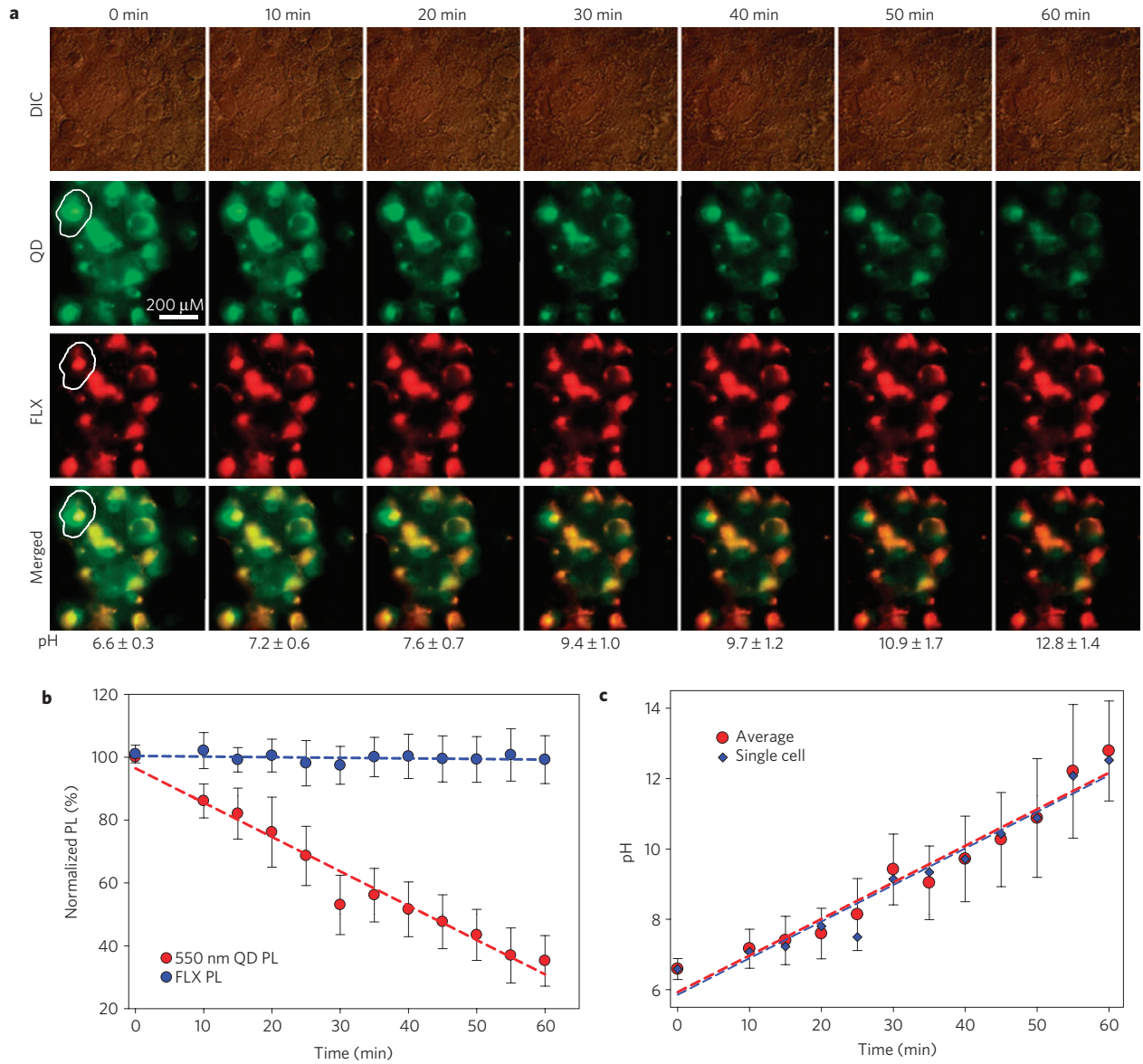

Figure 5 | Intracellular pH sensing. a, Differential interference contrast (DIC) and fluorescent micrographs collected from COS-1 cells co-injected with 550-nm-emitting QD–dopamine conjugates and FLX nanospheres in PBS at pH 6.5. Medium was switched to PBS at pH 11.5 supplemented with nystatin and micrographs were captured at the indicated time intervals from both the QD and FLX emission channels. Merged images are shown in the bottom row and pH values extracted at each time interval are shown below. **b**, QD and FLX PL intensities collected from the images shown in **a**, versus time, normalized to their values at $t = 0$; signals were averaged over $n = 18$ cells shown in this experiment. **c**, Average pH values derived from the PL data in **b**, using the calibration curve in Fig. 4b are shown along with those extracted from a single cell (outlined in **a**); linear fits are also shown. Good agreement between single cell and average values is observed. The 50 min time point exhibits the largest s.d. across all of the cells at ~16%.

Importantly, the linear correspondence between QD-conjugate quenching response and the change in dopamine–peptide E_f versus pH (see Fig. 4b) shows that both processes arise from the same electrochemistry. Although dopamine is partially deprotonated between the two dopamine pK_a values[22], we still observe a linear quenching response to pH 11.5. At pH values greater than or equal to the second dopamine pK_a value, rapid deprotonation will outcompete oxidation and may delineate the upper pH-sensing limit. Covalent dopamine attachment to peptides may extend the sensing range, as free dopamine reacts with its amine at higher pH, forming a cyclic/chain product (oxidative cyclization by Michael addition)[24,26]. Peptide self-assembly and the proximity provided between the nanocrystal and dopamine are also important for effective sensing. Consistent with short exponentially dependent distances expected for electron-transfer processes in conjunction with peptide propensity to act as an insulator[43], we note that quenching from low-valence configurations was negligible at almost all pH values. Efficient quenching requires multiple quinones to be arrayed around the QD to provide a higher probability of interaction; a configuration attained only at larger valences ($\geq$10 dopamine per QD, see Fig. 2) and basic pH.

QD–dopamine assemblies also provided an estimate of intracellular pH increases in cells. We began microinjecting conjugate solutions equilibrated to pH 6.5 in PBS and the initial pH value derived from the sensors is 6.6 ± 0.3. The pH 12.8 ± 1.4 value derived for the 60 min time point is only a ~10% difference from the expected pH 11.5 value. The plot in Fig. 5c shows data from monitoring a single cell (outlined in Fig. 5a) exhibiting excellent concordance with the averaged data confirming that single-cell resolution is achievable. Although it is unlikely that such pH

changes will be encountered in many biological environments, this format showed that QD conjugates could be introduced into cells and still sense broad pH ranges, confirming biocompatibility. Conjugates also transduced *in vitro* or intracellular pH decreases, although PL recovery was not linear or as dynamic in magnitude as the quenching observed with pH increases. We surmise that several factors contribute to this, including slower rates of quinone back conversion to hydroquinone (which requires two electrons and two protons), a lack of appropriate reductant and the complexity of the intracellular environments.

Owing to the similar configuration (CdSe/ZnS QDs functionalized with dopamine) used to achieve redox-sensitive cellular staining reported by Nadeau and co-workers[20], some comparison is warranted. A preliminary interpretation of that research suggested dopamine as an electron acceptor[44]; however, later reports consistently describe it as an electron donor to the QDs (refs 21,44,45). We find strong evidence for the quinone functioning as an electron acceptor. We demonstrate a clear dependence of quenching on QD size and consistent with this, they noted significantly more quenching for greener 560-nm QDs than yellow 590-nm QDs after dopamine conjugation[20], although they later found 'quenching data was quite unique for each QD and generally independent of size'[45]. We maintain finite control over dopamine valence and demonstrate consistent ratio-dependent effects, whereas dopamine numbers in their conjugates were only estimated and seem to be much higher, ~200–250 per QD (refs 20,21,45). pH is a critical factor in dopamine–QD interactions; however, this was not considered in their format. Although dopamine conjugation to QDs in both configurations initially results in quenching, they report PL increases under oxidizing conditions and constant ultraviolet excitation, whereas we observed no such result. They report PL increases on addition of millimolar β-mercaptoethanol (BME) reductant to nanomolar–micromolar QD–dopamine, whereas we found consistent PL decreases with BME regardless of pH or dopamine valence when attempting this format (data not shown). Some differences can be ascribed to chemistry. Our PEGylated dithiol ligands tolerate wide pH, have high-affinity for the QD surface and protect against competition from excess thiols[46,47], whereas their monothiol ligands have pH instability and poor long-term colloidal dispersibility[48,49]. Furthermore, using BME with QDs is notoriously complicated as it both acts as a surface ligand and alters the QD PL properties in a complex manner[50]. We do not directly include oxidants/reductants with the conjugates; we chemically predetermine the dopamine redox state on the peptide before QD assembly. Within our framework, alternative interpretations may be responsible for their observations. Banerjee *et al.* demonstrated that CdS:Mn/ZnS QDs could be quenched by capping with dopamine ligands and PL could be 'switched on' by adding similar millimolar concentrations of glutathione or dithiothreitol reductants that displaced the dopamine ligand[14]. Oxidized benzoquinones also undergo Michael addition with nucleophiles, including thiols such as BME, resulting in more than one nucleophile added to each quinone species, which abrogates redox properties[51–53]. This suggests direct cap-exchange of dopamine ligand or dopamine modification by BME (driven by excess) as possible explanations for their results. Electron-transfer-based QD sensors have been developed before and even extended to monitor intracellular glucose levels[54,55]. QD-based pH sensors have also been reported and typically exploit FRET and ratiometric analysis with proximal pH-dependent fluorophores[56–59]. Our approach extends these results, removes the need for spectral pairing with acceptor dyes and demonstrates that QD-based pH sensing can be applied intracellularly.

Methods

CdSe/ZnS core/shell QDs with emission maxima centred at ~520, 550 and 580 nm were made hydrophilic with PEG-modified dihydrolipoic acid (DHLA) ligands[46,60] (see Supplementary Fig. S1A). Dopamine–isothiocyanate (4-(2′-isothiocyanatoethyl)-1,2-benzenediol) was synthesized from dopamine and used to site-specifically label the unique N-terminal primary amine on the peptide NH_2-GSGAAAGLSH$_6$ (see Fig. 1a and Supplementary Information). This strategy also prevents dopamine cyclization by Michael addition at basic pH. Dopamine–peptide was reduced with 1% hydrazine in distilled-deionized H_2O (ref. 61), purified to remove reductant, quantitated, lyophilized and stored at −20 °C using a procedure similar to that described in ref. 62. Note, that pre-reduction is critical to later function, as it ensures that a sizeable fraction of the dopamines coupled to the QDs are initially in the reduced state (see above). We use metal-affinity coordination of polyhistidine-appended peptides to the ZnS surface of pH-stable PEGylated QDs as the basis for our conjugates. Benefits of this approach include: (1) obviating the multiple conjugation/purification steps needed for direct labelling of QD surface groups, (2) rapid assembly and high affinity/stability ($K_d^{-1} \sim 10^9$ M^{-1}), (3) control over the number of dopamine–peptides attached per QD through the molar ratio added and (4) providing dopamine proximity to the QD surface[63,64]. Comparison of this peptide to similar sequences where the QD core to peptide-terminus distance had been determined by FRET suggests that dopamine is located <10 Å from the QD surface when conjugated[63,64]. Dopamine–peptide stock solutions were resolubilized in 95:5 deionized H_2O/dimethylsulphoxide and self-assembled to QDs in deionized H_2O for ≥30 min as described[63,64]. QD–peptide stock solutions (0.2 μM) were aliquoted into PBS (137 mM NaCl, 10 mM phosphate, 2.7 mM KCl) preadjusted to the indicated pH values before fluorescence analysis.

Received 20 February 2010; accepted 22 June 2010; published online 23 July 2010

References

1. Michalet, X. *et al.* Quantum dots for live cells, *in vivo* imaging, and diagnostics. *Science* **307,** 538–544 (2005).
2. Klostranec, J. M. & Chan, W. C. W. Quantum dots in biological and biomedical research: Recent progress and present challenges. *Adv. Mater.* **18,** 1953–1964 (2006).
3. Shim, M., Wang, C. J. & Guyot-Sionnest, P. Charge-tunable optical properties in colloidal semiconductor nanocrystals. *J. Phys. Chem. B.* **105,** 2369–2373 (2001).
4. Anderson, N. A. & Lian, T. Q. Ultrafast electron transfer at the molecule-semiconductor nanoparticle interface. *Annu. Rev. Phys. Chem.* **56,** 491–519 (2005).
5. Raymo, F. M. & Yildiz, I. Luminescent chemosensors based on semiconductor quantum dots. *Phys. Chem. Chem. Phys.* **9,** 2036–2043 (2007).
6. Palaniappan, K., Hackney, S. A. & Liu, J. Supramolecular control of complexation-induced fluorescence change of water-soluble, beta-cyclodextrin-modified CdS quantum dots. *Chem. Commun.* 2704–2705 (2004).
7. Neuman, D. *et al.* Quantum dot fluorescence quenching pathways with Cr(III) complexes. Photosensitized NO production from trans-Cr(cyclam)(ONO)(2)(+). *J. Am. Chem. Soc.* **130,** 168–175 (2008).
8. Medintz, I. L. *et al.* Interactions between redox complexes and semiconductor quantum dots coupled via a peptide bridge. *J. Am. Chem. Soc.* **130,** 16745–16756 (2008).
9. Callan, J. F., Mulrooney, R. C., Kamila, S. & McCaughan, B. Anion sensing with luminescent quantum dots—a modular approach based on the photoinduced electron transfer (PET) mechanism. *J. Fluor.* **18,** 527–532 (2008).
10. Dayal, S. *et al.* Observation of non-Forster-type energy-transfer behavior in quantum dot-pthalocyanine conjugates. *J. Am. Chem. Soc.* **128,** 13974–13975 (2006).
11. Ruedas-Rama, M. J. & Hall, E. A. H. Azamacrocycle activated quantum dot for zinc ion detection. *Anal. Chem.* **80,** 8260–8268 (2008).
12. Gill, R., Zayats, M. & Willner, I. Semiconductor quantum dots for bioanalysis. *Angew. Chem. Int. Ed.* **47,** 7602–7625 (2008).
13. Gill, R. *et al.* Probing biocatalytic transformations with CdSe–ZnS QDs. *J. Am. Chem. Soc.* **128,** 15376–15377 (2006).
14. Banerjee, S., Kar, S., Perez, J. M. & Santra, S. Quantum dot-based OFF/ON probe for detection of glutathione. *J. Phys. Chem. C* **113,** 9659–9663 (2009).
15. Liu, X., Cheng, L. X., Lei, J. P. & Ju, H. X. Dopamine detection based on its quenching effect on the anodic electrochemiluminescence of CdSe quantum dots. *Analyst* **133,** 1161–1163 (2008).
16. Yuan, J., Guo, W., Yang, X. & Wang, E. Anticancer drug-DNA interactions measured using a photoinduced electron-transfer mechanism based on luminescent quantum dots. *Anal. Chem.* **81,** 362–368 (2009).
17. Uematsu, T., Waki, T., Torimoto, T. & Kuwabata, S. Systematic studies on emission quenching of cadmium telluride nanoparticles. *J. Phys. Chem. C* **113,** 21621–21628 (2009).
18. Lee, K. R. & Kang, I. J. Effects of dopamine concentration on energy transfer between dendrimer-QD and dye-labeled antibody. *Ultramicroscopy* **109,** 894–898 (2008).

19. Palaniappan, K., Xue, C. H., Arumugam, G., Hackney, S. A. & Liu, J. Water-soluble, cyclodextrin-modified CdSe–CdS core–shell structured quantum dots. *Chem. Mater.* **18,** 1275–1280 (2006).
20. Clarke, S. J. *et al.* Photophysics of dopamine-modified quantumdots and effects on biological systems. *Nature Mater.* **5,** 409–417 (2006).
21. Cooper, D. R. *et al.* Photoenhancement of lifetimes in CdSe/ZnS and CdTe quantum dot–dopamine conjugates. *Phys. Chem. Chem. Phys.* **11,** 4298–4310 (2009).
22. Laviron, E. Electrochemical reactions with protonations at equilibrium. 10. The kinetics of the parabenzoquinone hydroquinone couple on a platinum-electrode. *J. Electroanal. Chem.* **164,** 213–227 (1984).
23. Wraight, C. A. Proton and electron transfer in the acceptor quinone complex of photosynthetic reaction centers from Rhodobacter sphaeroides. *Front. Biosci.* **9,** 309–337 (2004).
24. Patai, S. & Rappoport, Z. *The Chemistry of the Quinonoid Compounds, Part I & II* (John Wiley, 1988).
25. Finklea, H. O. Theory of coupled electron–proton transfer with potential-dependent transfer coefficients for redox couples attached to electrodes. *J. Phys. Chem. B* **105,** 8685–8693 (2001).
26. Klegeris, A., Korkina, L. G. & Greenfield, S. A. Autoxidation of dopamine—a comparison of luminescent and spectrophotometric detection in basic solutions. *Free Radic. Biol. Med.* **18,** 215–222 (1995).
27. Laitinen, H. A. & Harris, W. E. *Chemical Analysis: An Advanced Text and Reference* 2nd edn (McGraw-Hill, 1975).
28. Bailey, S. I. & Ritchie, I. M. A cyclic voltammetric study of the aqueous electrochemistry of some quinones. *Electrochim. Acta* **30,** 3–12 (1985).
29. Costentin, C. Electrochemical approach to the mechanistic study of proton-coupled electron transfer. *Chem. Rev.* **108,** 2145–2179 (2008).
30. Hay, S., Westerlan, K. & Tommow, C. Redox characteristics of a de novo quinone protein. *J. Phys. Chem. C* **111,** 3488–3495 (2007).
31. Prasuhn, D. E. *et al.* Polyvalent display and packing of peptides and proteins on semiconductor quantum dots: Predicted versus experimental results. *Small* **6,** 555–564 (2010).
32. Wang, H. Y., Sun, Y. & Tang, B. Study on fluorescence property of dopamine and determination of dopamine by fluorimetry. *Talanta* **57,** 899–907 (2002).
33. Mancini, M. C., Kairdolf, B. A., Smith, A. M. & Nie, S. M. Oxidative quenching and degradation of polymer-encapsulated quantum dots: New insights into the long-term fate and toxicity of nanocrystals *in vivo*. *J. Am. Chem. Soc.* **130,** 10836–10837 (2008).
34. Yuan, J., Guo, W. & Wang, E. Utilizing a CdTe quantum dots-enzyme hybrid system for the determination of both phenolic compounds and hydrogen peroxide. *Anal. Chem.* **80,** 1141–1145 (2008).
35. Liu, X. & Ju, H. X. Coreactant enhanced anodic electrochemiluminescence of CdTe quantum dots at low potential for sensitive biosensing amplified by enzymatic cycle. *Anal. Chem.* **80,** 5377–5382 (2008).
36. Schumb, W. C. Stability of concentrated hydrogen peroxide solutions. *Ind. Eng. Chem.* **41,** 992–1003 (1949).
37. Korn, S. J. & Horn, R. Influence of sodium–calcium exchange on calcium current rundown and the duration of calcium-dependent chloride currents in pituitary cells, studied with whole cell and perforated patch recording. *J. Gen. Physiol.* **94,** 789–812 (1989).
38. Medintz, I. L. & Mattoussi, H. Quantum dot-based resonance energy transfer and its growing application in biology. *Phys. Chem. Chem. Phys.* **11,** 17–45 (2009).
39. Burda, C., Green, T. C., Link, S. & El-Sayed, M. A. Electron shuttling across the interface of CdSe nanoparticles monitored by femtosecond laser spectroscopy. *J. Phys. Chem. B* **103,** 1783–1788 (1999).
40. Yarovoi, A. A. *et al.* Photo-induced electron transfer in CdSe nanocrystals passivated by quinone derivatives. *Proc. SPIE* **6728,** 67282K (2007).
41. Lou, Y. B., Chen, X. B., Samia, A. C. & Burda, C. Femtosecond spectroscopic investigation of the carrier lifetimes in digenite quantum dots and discrimination of the electron and hole dynamics via ultrafast interfacial electron transfer. *J. Phys. Chem. B* **107,** 12431–12437 (2003).
42. Long, D., Wu, G., Wang, W. & Yao, S. Photo-induced interfacial electron transfer from CdSe quantum dots to surface-bound p-benzoquinone and anthraquinone. *Res. Chem. Intermed.* **33,** 655–661 (2007).
43. Marcus, R. A. & Sutin, N. Electron transfers in chemistry and biology. *Biochim. Biophys. Acta* **811,** 265–322 (1985).
44. Clarke, S. J. *Synthesis, Biological Targeting and Photophysics of Quantum Dots*, Ch. 6. Ph.D. thesis. Department of Biomedical Engineering, McGill University (2008).
45. Clarke, S. J., Hollmann, C. A., Aldaye, F. A. & Nadeau, J. L. Effect of ligand density on the spectral, physical, and biological characteristics of CdSe/ZnS quantum dots. *Bioconjugate Chem.* **19,** 562–568 (2008).
46. Mei, B. C. *et al.* Modular poly(ethylene glycol) ligands for biocompatible semiconductor and gold nanocrystals with extended pH and ionic stability. *J. Mater. Chem.* **18,** 4949–4958 (2008).
47. Mei, B. C. *et al.* Effects of ligand coordination number and surface curvature on the stability of gold nanoparticles in aqueous solutions. *Langmuir* **25,** 10604–10611 (2009).
48. Aldana, J., Lavelle, N., Wang, Y. J. & Peng, X. G. Size-dependent dissociation pH of thiolate ligands from cadmium chalcogenide nanocrystals. *J. Am. Chem. Soc.* **127,** 2496–2504 (2005).
49. Parak, W. J. *et al.* Biological applications of colloidal nanocrystals. *Nanotechnology.* **14,** R15–R27 (2003).
50. Jeong, S. *et al.* Effect of the thiol–thiolate equilibrium on the photophysical properties of aqueous CdSe/ZnS nanocrystal quantum dots. *J. Am. Chem. Soc.* **127,** 10126–10127 (2005).
51. Cai, P. & Snyder, J. K. Preparation, reactivity and neurotoxicity of tryptamine-4,5-dione. *Tetrahedron Lett.* **31,** 969–972 (1990).
52. Shamsipur, M., Kazemi, S. H., Alizadeh, A., Mousavi, M. F. & Workentin, M. S. Self-assembled monolayers of a hydroquinone-terminated alkanethiol onto gold surface. Interfacial electrochemistry and Michael-addition reaction with glutathione. *J. Electroanal. Chem.* **610,** 218–226 (2007).
53. Huang, X., Xu, R., Hawley, M. D., Hopkins, T. L. & Kramer, K. J. Electrochemical oxidation of *n*-acyldopamines and regioselective reactions of their quinones with *n*-acetylcysteine and thiourea. *Arch. Biochem. Biophys.* **352,** 19–30 (1998).
54. Freeman, R. *et al.* Biosensing and probing of intracellular metabolic pathways by NADH-sensitive quantum dots. *Angew. Chem. Int. Ed.* **48,** 309–313 (2009).
55. Freeman, R. & Willner, I. NAD(+)/NADH-sensitive quantum dots: Applications to probe NAD(+)-dependent enzymes and to sense the RDX explosive. *Nano Lett.* **9,** 322–326 (2009).
56. Tomasulo, M., Yildiz, I. & Raymo, F. M. pH-sensitive quantum dots. *J. Phys. Chem. B* **110,** 3853–3855 (2006).
57. Snee, P. T. *et al.* A ratiometric CdSe/ZnS nanocrystal pH sensor. *J. Am. Chem. Soc.* **128,** 13320–13321 (2006).
58. Chen, Y., Thakar, R. & Snee, P. T. Imparting nanoparticle function with size-controlled amphiphilic polymers. *J. Am. Chem. Soc.* **130,** 3744–3745 (2008).
59. Zhang, F. *et al.* Ion and pH sensing with colloidal nanoparticles: Influence of surface charge on sensing and colloidal properties. *ChemPhysChem* **11,** 730–735 (2010).
60. Dabbousi, B. O. *et al.* (CdSe)ZnS core–shell quantum dots: Synthesis and optical and structural characterization of a size series of highly luminescent materials. *J. Phys. Chem. B* **101,** 9463–9475 (1997).
61. Aziz, M. Z., Selvaraju, T. & Yang, H. Selective determination of catechol in the presence of hydroquinone at bare indium tin oxide electrodes via peak-potential separation and redox cycling by hydrazine. *Electroanalysis* **14,** 1543–1546 (2007).
62. Sapsford, K. E. *et al.* Monitoring of enzymatic proteolysis on a electroluminescent-CCD microchip platform using quantum dot–peptide substrates. *Sens. Actuat. B* **139,** 13–21 (2009).
63. Sapsford, K. E. *et al.* Kinetics of metal-affinity driven self-assembly between proteins or peptides and CdSe–ZnS quantum dots. *J. Phys. Chem. C* **111,** 11528–11538 (2007).
64. Medintz, I. L. *et al.* Proteolytic activity monitored by fluorescence resonance energy transfer through quantum-dot–peptide conjugates. *Nature Mater.* **5,** 581–589 (2006).

Acknowledgements

The authors thank T. O'Shaughnessy and I. Willner for helpful suggestions and acknowledge the CB Directorate/Physical S&T Division (DTRA), ONR, NRL and the NRL-NSI for financial support. M.H.S. acknowledges an NRC fellowship through NRL. J.B.B-C. acknowledges a Marie Curie International Outgoing Fellowship.

Author contributions

I.L.M., M.H.S. and S.A.T. conceived of the experimental strategy and carried out experiments. J.B.B-C. and P.E.D. designed and synthesized the peptides used. K.S., B.C.M. and M.H.S. synthesized QD material. M.H.S. synthesized the dopamine isothiocyante. K.S. and H.M. analysed experimental results. J.B.D. grew cell cultures and assisted with cellular experiments. J.S.M. carried out fluorescence lifetime experiments.

Additional information

The authors declare no competing financial interests. Supplementary information accompanies this paper on www.nature.com/naturematerials. Reprints and permissions information is available online at http://npg.nature.com/reprintsandpermissions. Correspondence and requests for materials should be addressed to I.L.M.